eprints@whiterose.ac.uk
https://eprints.whiterose.ac.uk/

Accepted Article

RESEARCH ARTICLE

New Radical Route and Insight for Highly Efficient Benzimidazoles Synthesis Integrated with Hydrogen Evolution

Yin-Feng Wang,[1] Ming-Yu Qi,[1] Marco Conte,[2] Zi-Rong Tang,[1] and Yi-Jun Xu[1],*

[1]   Y.-F. Wang, M.-Y. Qi, Prof. Dr. Z.-R. Tang, Prof. Dr. Y.-J. Xu
       College of Chemistry, State Key Laboratory of Photocatalysis on Energy and Environment, Fuzhou University, Fuzhou 350116 (China)
       E-mail: yjxu@fzu.edu.cn
       Homepage: http://xugroup.fzu.edu.cn
[2]   Dr. M. Conte
       Department of Chemistry, University of Sheffield, Sheffield, S3 7HF, (UK)

       Supporting information for this article is given via a link at the end of the document.

Abstract: Benzimidazoles are a versatile class of scaffolds with important biological activities, whereas their synthesis in a lower-cost and more efficient manner remains a challenge. Here, we demonstrate a conceptually new radical route for the high-performance photoredox coupling of alcohols and diamines to synthesize benzimidazoles along with stoichiometric hydrogen (H_2) over Pd-decorated ultrathin ZnO nanosheets (Pd/ZnO NSs). Mechanistic study reveals the unique advantage of ZnO NSs over other supports and particularly that the features of Pd nanoparticles in facilitating the cleavage of the α-C−H bond of alcohols and adsorbing subsequently-generated C−centered radicals hold the key to turning on the reaction. This work highlights a new insight into radical-induced efficient benzimidazoles synthesis pairing with H_2 evolution by rationally designing semiconductor-based photoredox systems.

Introduction

The ubiquity of benzimidazoles in pharmaceuticals and agrochemicals for the treatment of infections and for crop protection respectively, has stimulated numerous efforts toward their synthesis over the past decades.[1] Typically, benzimidazoles are synthesized *via* the coupling between *o*-arylenediamines and carboxylic acids or their derivatives with strong acids and elevated temperature, which however generate a large number of by-products.[2] Additionally, benzimidazoles can also be synthesized by the condensation of *o*-arylenediamines with aldehydes, but stoichiometric or excessive and undesired strong oxidants (oxone,[3] DDQ,[4] or Pb(OAc)[5]) are required. Under such circumstances, alternative methods that proceed under mild reaction conditions for economically and environmentally benign benzimidazoles synthesis are highly desired to avoid the harsh reaction conditions, huge energy consumption and poor product selectivity of traditional benzimidazoles synthesis methods.

A recent development for photoredox-catalyzed organic synthesis using renewable solar energy and semiconductor photocatalysts, represents a promising method for benzimidazoles synthesis.[6] Since Shiraishi and co-workers first reported the photocatalytic synthesis of benzimidazoles *via* the cross-coupling between *o*-arylenediamines and alcohols over a Pt-loaded TiO_2 photocatalyst in 2009,[7] semiconductor-based photocatalytic systems for benzimidazoles synthesis have been

extensively studied.[8] Given that alcohols are more stable and readily available from naturally abundant carbon sources, using alcohols with *o*-arylenediamines to synthesize benzimidazoles is highly desirable. Generally, the reaction between alcohols and *o*-arylenediamines to produce benzimidazoles requires oxidative dehydrogenation of alcohols to form aldehyde intermediates followed by condensing with *o*-arylenediamines for finally benzimidazoles production.[7, 9] However, this conventional route of benzimidazoles synthesis has a potential drawback, in which the accumulation of aldehyde intermediates may lead to the generation of undesirable by-products, thereby resulting in the low selectivity of the desired benzimidazole.[7, 10] In such a scenario, developing new synthetic routes to achieve more efficient benzimidazoles synthesis remains an aspirational target. Due to the advantages of high yield, mild reaction conditions and great functional group compatibility in organic synthesis brought by the high chemical reactivity of free radicals,[11] the alternative routes, utilizing radicals generated from alcohols as active intermediates to trigger the reaction is an ideal but yet-to-be-realized concept for the efficient benzimidazoles synthesis. Nevertheless, the selective activation of targeted bonds in alcohols with complex chemical linkages (C−C, α/β-C−H, C−O, and O−H) to generate designated radical intermediates is of great challenge, which requires the well-defined catalyst with definite catalytically active sites.[12] The premise of constructing C−heteroatom bonds of benzimidazoles is the prioritized C−H bond scission.[13] Therefore, it is highly important to rationally develop photocatalysts, which could effectively cleave the C−H bond in alcohols for C−centered radicals generation.

In light of the above principle, constructing two-dimensional ZnO nanosheets (NSs) based composite photocatalyst could be a potential approach. In fact, the open and accessible surface of ZnO NSs facilitates the exposure of active sites,[14] and the abundant Zn^+−O^- pairs could efficiently activate the α-C−H and O−H bonds of alcohols,[15] thus allowing ZnO available for the radical formation if upon UV irradiation. Despite pristine ZnO suffers from the rapid electron-hole recombination resulting in limited photocatalytic efficiency,[16] surface modification of ZnO with metal (*e.g.*, Au, Ag, Pd) cocatalysts is an effective route to overcome this inherent obstacle by adjusting interface redox kinetics and accelerating charge separation.[17] Particularly, Pd species have been reported to contribute to the preferential breakage of α-C−H bond of alcohols.[18] In this context, it could be expected that the ingenious integration of ZnO NSs to bind an

RESEARCH ARTICLE

alcohol species with sufficiently exposed surface and Pd cocatalyst to operate a selective C−H cleavage could be an appealing strategy for high-performance benzimidazoles synthesis *via* the radical route.

Herein, we for the first time report a conceptually new, highly efficient radical route for the benzimidazoles synthesis *via* radical-induced cross-coupling of alcohols and *o*-arylenediamines concomitantly with hydrogen (H_2) production over Pd modified ultrathin ZnO NSs (Pd/ZnO) under mild conditions. Our methodology directly uses high-reactive C−centered radicals generated from alcohols to initiate the cross-coupling reaction, bypassing the aldehyde intermediates as widely reported in previous works,[7, 9] as well as simultaneously producing H_2 as solar fuel, thereby featuring a high atom-economy. Our mechanistic studies reveal that the introduction of Pd nanoparticles not only facilitates the photogenerated charge separation, but also supplies active sites for the cleavage of the α-C−H bond of alcohols and adsorbing subsequently-generated C−centered radicals. Density functional theory (DFT) calculations illustrate that the C-centered radicals adsorbed on Pd are more likely to directly attack the *o*-arylenediamines adsorbed on the Lewis acid sites of Pd/ZnO to finally generate benzimidazoles rather than *via* aldehyde intermediates, leading to a new radical reaction pathway for the benzimidazoles synthesis.

Results and Discussion

The overall fabrication procedure of Pd-decorated ultrathin ZnO nanosheets (NSs) composites (Pd/ZnO) is schematically sketched in **Figure 1a**. Initially, ultrathin ZnO NSs have been prepared *via* a hydrolysis method (**Figure 1a**). The thickness of ZnO NSs is determined to be *ca.* 0.85 nm by atomic force microscopy (AFM, **Figure 1b** and **1c**), which roughly corresponds to one unit cell of hexagonal wurtzite ZnO.[19] Subsequently, Pd nanoparticles (NPs) are loaded onto the surface of ZnO NSs by the photodeposition method to finally obtain Pd/ZnO composites with different contents of Pd. The actual content of Pd in the samples has been measured by inductively coupled plasma atomic emission spectroscopy (ICP-AES, **Table S1**). As observed from the transmission electron microscopy (TEM) images (**Figure 1d** and **Figure S1**), the similar sheet structures of ZnO and Pd/ZnO composites indicate that Pd deposition does not change the morphology of ZnO. The Pd NPs size of all samples is in the range of 2.5 to 3.2 nm (**Figure S1**), meaning that it is not affected by the amount of Pd loading though this is ranging from 1 to 20 wt%, thus implying highly dispersed nanoparticles within this loading range. In **Figure 1e**, the two well-defined lattice fringes with d-spacing of 0.23 and 0.26 nm, corresponding to the (111) plane of Pd NPs and (001) crystal facet of ZnO, respectively.[20]
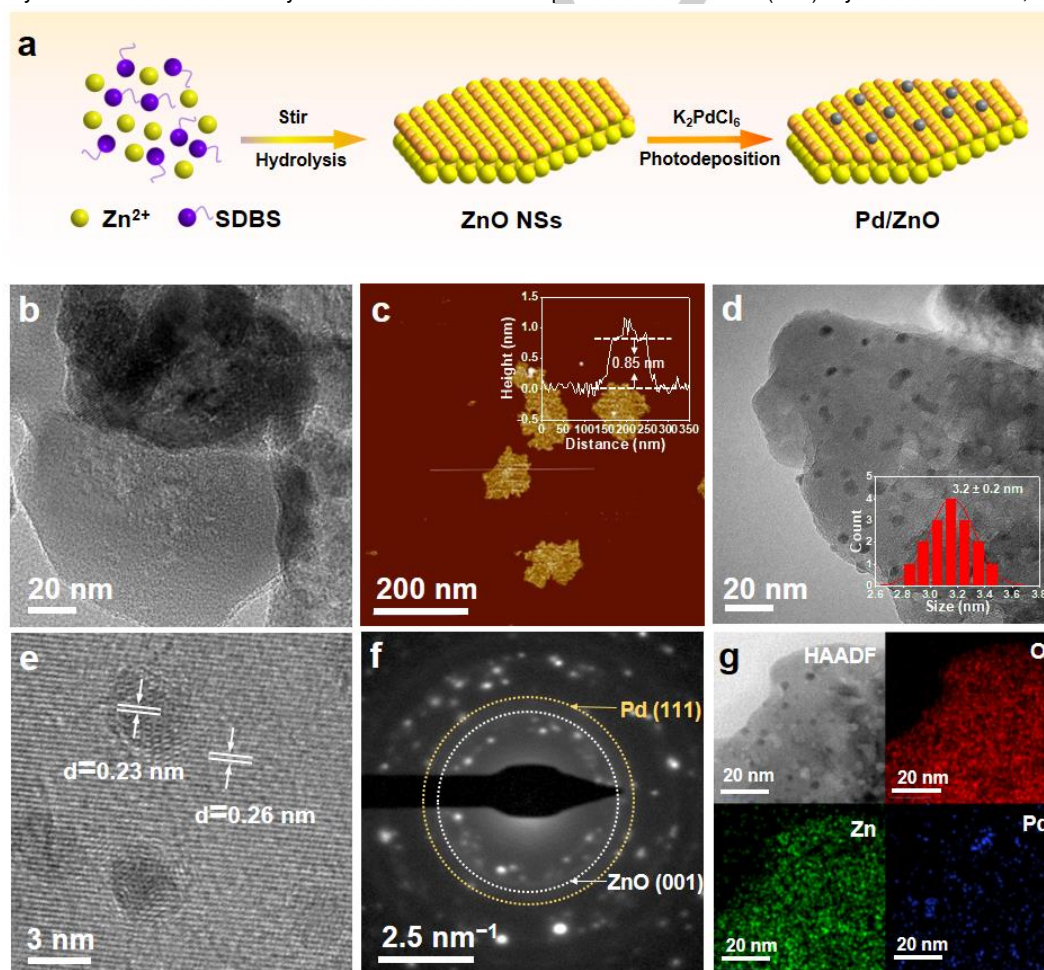
Figure 1. (a) Schematic illustration for the synthesis of the Pd/ZnO composites. (b) TEM image of ZnO NSs. (c) AFM image of the ZnO NSs (inset is the corresponding height profile of the ZnO NSs). (d-f) TEM image, HRTEM image and SAED image of 15Pd/ZnO. (g) HAADF-STEM image and the elemental mapping results of 15Pd/ZnO. The inset of (d) is the particle size diagram of 15Pd/ZnO.

RESEARCH ARTICLE

The corresponding selected area electron diffraction (SAED) image (**Figure 1f**) exhibits that the index of the concentric rings is consistent with the Pd (111) and ZnO (001) facets, revealing the polycrystalline nature of 15Pd/ZnO (where 15 stands for the wt% of Pd in this sample).[20b, 21] High-angle annular dark field-scanning TEM (HAADF-STEM) image and elemental mapping (**Figure 1g**) confirm the uniform distribution of Zn, O, and Pd elements in 15Pd/ZnO.

The chemical element compositions and valence states of samples have been analyzed by X-ray photoelectron spectroscopy (XPS). In the survey XPS spectrum (**Figure S2a**), the coexistence of Pd, Zn, and O elements in 15Pd/ZnO is accordance with the aforementioned elemental mapping results. In **Figure 2a**, the peak at 530.30 eV is attributed to the lattice oxygen (O_L) in ZnO and the peak at 531.33 eV is assigned to the chemisorbed oxygen.[16a, 22] Notably, the O_L characteristic peak position of 15Pd/ZnO does not change compared with pristine ZnO, implying the loading of Pd NPs does not destroy the lattice structure of ZnO. In the Pd 3d spectra (**Figure 2b**), the fitted double peaks with binding energies of 335.38 and 340.64 eV belong to $3d_{5/2}$ and $3d_{3/2}$ orbitals of Pd^0, respectively, and the two peaks located at 336.28 and 341.54 eV are ascribed to $3d_{5/2}$ and $3d_{3/2}$ orbitals of Pd^{2+} due to the inevitable oxidation of Pd NPs surface.[21, 23] All of these XPS results further confirm that Pd NPs and ZnO have been successfully combined.

X-ray diffraction (XRD) has been performed to identify the crystal phase structure of samples. As displayed in **Figure 2c**, the main diffraction characteristic peaks at 2θ values of 31.8°, 34.4° 36.3°, 47.5°, 56.6°, 62.9° and 67.9° are respectively indexed to (100), (002), (101), (102), (110), (103) and (112) crystallographic planes of hexagonal wurtzite ZnO (PDF#36-1451). After loading Pd NPs, an additional diffraction peak at 40.1°, which is indexed to the (111) plane of Pd NPs (PDF#88-2335) appears, manifesting the successful construction of 15Pd/ZnO composite.

The optical absorption properties of pristine ZnO and Pd/ZnO composites have been measured by ultraviolet-visible (UV-vis) diffuse reflectance spectroscopy (DRS). As shown in **Figure 2d**, pristine ZnO exhibits the obvious absorption in the ultraviolet band with an absorption edge at *ca.* 385 nm, which is consistent with the intrinsic band gap absorption of ZnO (**Figure S3a**).[24] Furthermore, the light absorption intensity of Pd/ZnO composites in the range of 400-750 nm significantly increases, demonstrating that Pd deposition is beneficial to enhance the light response of samples.[25]

The surface acid strength of samples has been determined by temperature programmed desorption of ammonia (NH_3-TPD). As presented in **Figure 2e**, the desorption peaks at around 120 °C are ascribed to NH_3 molecule adsorbed on the weak acid sites of samples.[26] Pyridine adsorption infrared spectra (Py-IR spectra) have been used to distinguish Lewis and Brønsted acid sites on the samples, as shown in **Figure 2f**. The adsorption band at around 1450 cm^{-1} arises from pyridine adsorbed on Lewis acid sites, and the band at around 1490 cm^{-1} is ascribed to pyridine adsorbed on both Brønsted and Lewis acid sites, indicating the coexistence of Brønsted and Lewis acid sites on the surface of samples.[27] As summarized in **Table S2**, the ratio of Brønsted and Lewis acid sites (B/L) is close to 0, revealing that Lewis acid sites dominate the surface of ZnO and 15Pd/ZnO. In addition, the total surface acidity of 15Pd/ZnO is only slightly decreased to 58 from 66 µmol g^{-1}, implying that the presence of Pd NPs has a negligible influence on the total amount of acid sites.

After recognizing the physicochemical properties of prepared samples, we are now in a position to evaluate their applicability in the photoredox-driven coproduction of 2-methylbenzimidazole (2MBZ) and hydrogen (H_2) by utilizing *o*-phenylenediamine (OPD) and ethanol as starting materials in argon (Ar) atmosphere (**Figure 3a**). As shown in **Figure 3b**, no gas and liquid products are detected over pristine ZnO, while the photocatalytic activity of
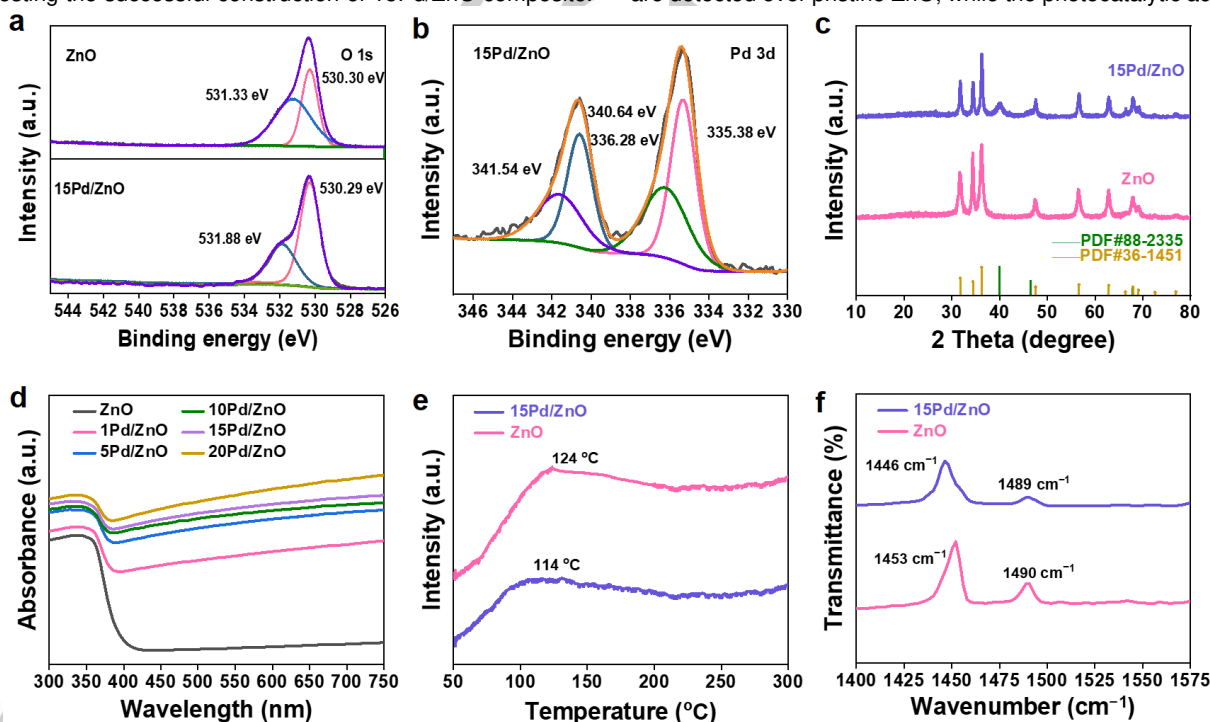

Figure 2. (a) High-resolution XPS spectra of O 1s of ZnO and 15Pd/ZnO. (b) High-resolution XPS spectra of Pd 3d of 15Pd/ZnO. (c) XRD patterns of ZnO and 15Pd/ZnO. (d) DRS spectra of ZnO and Pd/ZnO composites with different contents of Pd. (e) NH_3-TPD profiles and (f) Py-IR spectra of ZnO and 15Pd/ZnO.

RESEARCH ARTICLE

the Pd/ZnO composites is significantly increased due to the Pd NPs deposition. Specifically, 15Pd/ZnO exhibits the optimal catalytic performance (1.2 mmol g^{-1} h^{-1} of 2MBZ and 2.5 mmol g^{-1} h^{-1} of H_2) with high selectivity (98%), outperforming previously reported photocatalysts under similar conditions up to nearly an order of magnitude (**Table S3**). The yields toward the 2MBZ production of the prepared samples shown in **Figure 3b** imply the strong correlation of the 2MBZ production with Pd modification, confirming the critical role of Pd in such a reaction (**Figure S4**). According to the stoichiometric ratio of the 2MBZ and H_2, the ratio of electrons and holes consumed in the redox reaction is calculated to be *ca.* 1.0, indicating that the process is a stoichiometric dehydrogenation reaction.[28] In **Figure 3c**, the time-dependent analysis for 2MBZ and H_2 production over 15Pd/ZnO shows the continuous generation of 2MBZ and H_2 along with the extension of illumination time. As shown in **Figure 3d**, the activity of 15Pd/ZnO does not show a significant decrease after five cycles of testing. Moreover, the result of ICP spectroscopy analysis evidences that there is slightly detectable Pd^{2+} (7.68 µg, corresponding to 0.512% of leaching ratio) leakage over 15Pd/ZnO in the reaction solution (**Table S4**). These results indicate the great stability and recyclability of 15Pd/ZnO.

For comparison, commercial ZnO (c-ZnO) has been modified with the same photodeposition method to obtain 15Pd/c-ZnO (**Figure S5**), with the inhomogeneous size distribution of Pd NPs on the irregular c-ZnO surface. The average size of Pd NPs of 15Pd/c-ZnO (8.9 nm) is nearly three times that of 15Pd/ZnO (3.2 nm), indicating the poor dispersion of Pd NPs on c-ZnO surface.

Py-IR characterization (**Figure S6a** and **Table S2**) shows that the 15Pd/c-ZnO surface is also dominated by Lewis acid sites and the total acidity (38 µmol g^{-1}) is less than that of 15Pd/ZnO (58 µmol g^{-1}), consistent with the decline of c-ZnO (45 µmol g^{-1}) over ZnO NSs (66 µmol g^{-1}). The Brunauer-Emmett-Teller (BET) test (**Table S5**) shows that the surface area of 15Pd/ZnO (48 m²/g) is three times more than that of 15Pd/c-ZnO (15 m²/g), indicating that the large specific surface area of 15Pd/ZnO allows sufficient exposure of the Lewis acid sites and facilitates the homogeneous dispersion of the Pd NPs. As shown in **Figure 3e**, both gas and liquid products yield of 15Pd/c-ZnO decreases by approximately 33%, which might mainly be attributed to the reduction of acidic sites (approximately 34%) resulting in unfavorable adsorption of OPD, despite the different distribution and size of Pd NPs. Furthermore, previous work has demonstrated that the presence of molecular oxygen (O_2) can promote such dehydrogenation reactions.[29] Nevertheless, in the current system, the yield of 2MBZ in O_2 atmosphere is similar to that in the Ar atmosphere, and no H_2 production. This signifies that our system in the Ar atmosphere can simultaneously produce clean energy H_2, exhibiting the high atom-economy without compromising the yield of 2MBZ. When ethanol is replaced by acetaldehyde as the substrate, the 2MBZ yield of 15Pd/ZnO decreases by approximately 77%, and no by-products are detected. According to the 2MBZ synthesis mechanism in previous works,[7, 9d, 9e] if ethanol is converted directly to acetaldehyde, once the acetaldehyde is directly used as the substrate, the yield of 2MBZ should be greatly increased because of the simplification of the
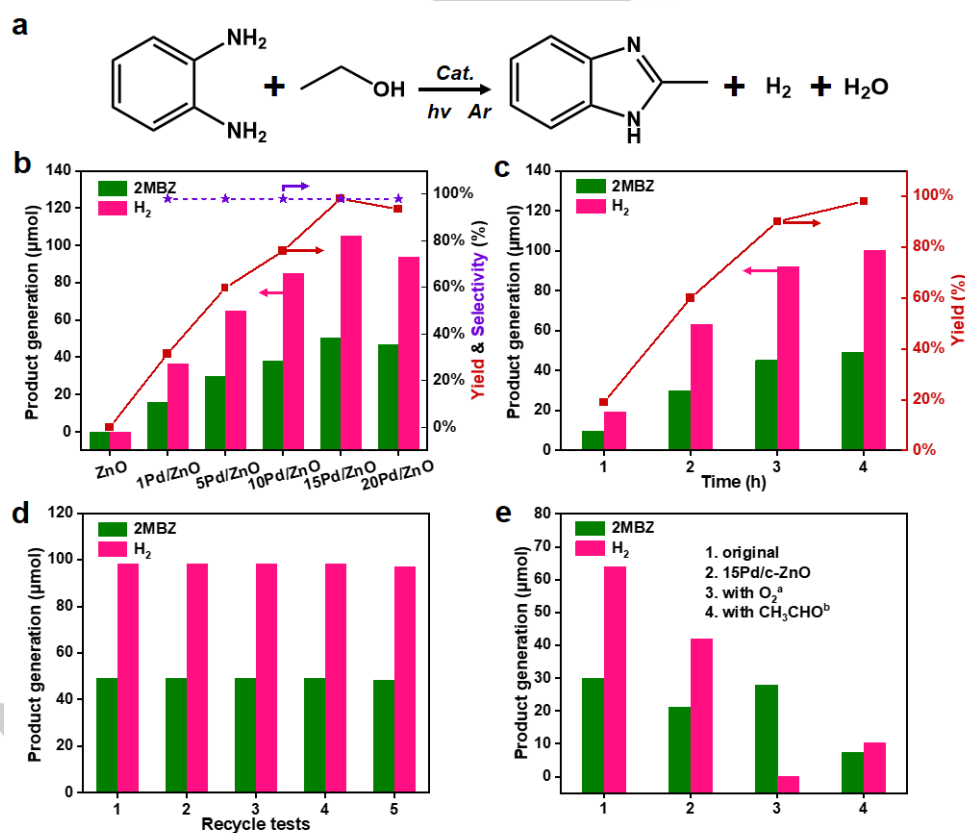
Figure 3. (a) Formula for the cross-coupling of OPD and ethanol. (b) Photocatalytic performance over pristine ZnO and Pd/ZnO composites with different contents of Pd after 4 h of illumination. (c) Time-dependent analysis over 15Pd/ZnO. (d) Recycle tests of 15Pd/ZnO. (e) Photocatalytic performance of comparative experiments under different experimental conditions after 2 h of illumination. [a]Reaction conditions: O_2 (1 atm). [b]0.25 mmol acetaldehyde dispersed in 10 mL acetonitrile solution.

4

Table 1. Summary of the production of benzimidazoles from different *o*-arylenediamines and alcohols over 15Pd/ZnO.[a]

Entry	Diamine	Alcohol	Liquid Product	Liquid Product Generation (μmol)	Liquid Product Yield (%)	H_2 Generation (μmol)	e−/h+[b]
1		CH_3OH		14.6	29.2	38.1	1.3
2				26.2	52.4	70.6	1.3
3				23.6	47.2	53.6	1.1
4				6.2	12.4	177	1.2[c]
5				49.6	99.2	89.9	0.9
6				44.2	88.4	70.6	0.8
7				49.8	99.6	78.5	0.8
8				4.7	9.4	28.1	3
9				trace	–	trace	–

[a]Reaction conditions: catalyst (10 mg), diamine (50 μmol), alcohol (10 mL), Ar (1 atm), Xe lamp (320 nm < λ < 780 nm), 4 h. [b]e−/h+ = n_{H_2}/2$n_{benzimidazoles}$. [c]e−/h+ = n_{H_2}/(2$n_{benzimidazoles}$+n_{BAD}).

reaction steps. However, the experimental results are contrary to the hypothesis. Moreover, it is noteworthy that a large amount of H_2 (173 μmol) and acetaldehyde (170 μmol) are produced in pure ethanol without OPD after 2 h of illumination, in which the yield of H_2 is nearly three times that of our reaction system (**Figure S7**). These results indicate that ethanol does not interact with OPD by acetaldehyde intermediate in the present catalytic system.

Various alcohols and *o*-arylenediamines with different substituent groups on aryl rings have been selected to evaluate the compatibility of our present photoredox system, as shown in **Table 1** (see **Figures S8** and **S9** for the mass spectra). Among the investigated aliphatic alcohols, the yields of corresponding benzimidazoles are related to their carbon chain length due to the different C−H activation strengths of various aliphatic alcohols.[30] However, the yield of H_2 is far higher than that of the corresponding benzimidazole when benzyl alcohol is used as the substrate. On the one hand, the steric hindrance effect hampers the corresponding benzimidazole synthesis.[31] The conversion of benzyl alcohol to benzaldehyde (BAD) and a small amount of C−C coupling products leads to a large amount of H_2 production. It is worth noting that the electronegativity of the functional group on the aromatic ring of OPD affects the yield of the corresponding benzimidazole. For the case of OPD with an electron-donating group (−OCH₃, entry 7 in **Table 1**), a considerable yield of the corresponding benzimidazole is obtained. In contrast, the conversion of *o*-arylenediamines with an electron-withdrawing group (−Cl) is significantly reduced (entry 8 in **Table 1**), and the

introduction of a −CN group (entry 9 in **Table 1**) even completely suppresses the corresponding benzimidazole formation.

To determine the photogenerated charge separation/transfer of samples, the photoelectrochemical characterizations, steady-state photoluminescence (PL) spectroscopy and time-resolved photoluminescence (TRPL) spectroscopy have been systematically performed. The electrochemical impedance spectroscopy (EIS) spectra (**Figure 4a**) shows that the Nyquist plot of 15Pd/ZnO has a smaller semicircle in contrast to ZnO, indicating a lower resistance and a greater charge carrier transfer rate between 15Pd/ZnO and electrolyte.[32] In **Figure 4b**, the transient photocurrent response of 15Pd/ZnO is higher than that of ZnO under intermittent light irradiation, demonstrating the higher charge separation efficiency in 15Pd/ZnO.[33] The steady-state PL intensity of 15Pd/ZnO is significantly less than that of ZnO, implying that the recombination of photogenerated electron-hole pairs is effectively suppressed (**Figure 4c**).[34] Following the fitting of the TRPL curves of **Figure S10** (**Table S6**), the emission lifetime of 15Pd/ZnO (7.3 ns) is less than that of pristine ZnO (22.8 ns), proving that faster interfacial charge transfer occurs in 15Pd/ZnO.[35] The above results together verify that the presence of Pd NPs expedites the separation/transfer of photogenerated charge carriers.

To decipher the reaction mechanism for 2MBZ formation in the present photocatalytic system, a series of control experiments have been carried out, as displayed in **Figure 4d**. In the absence of light or catalysts, the reaction cannot proceed at all. The

5

WILEY-VCH

RESEARCH ARTICLE
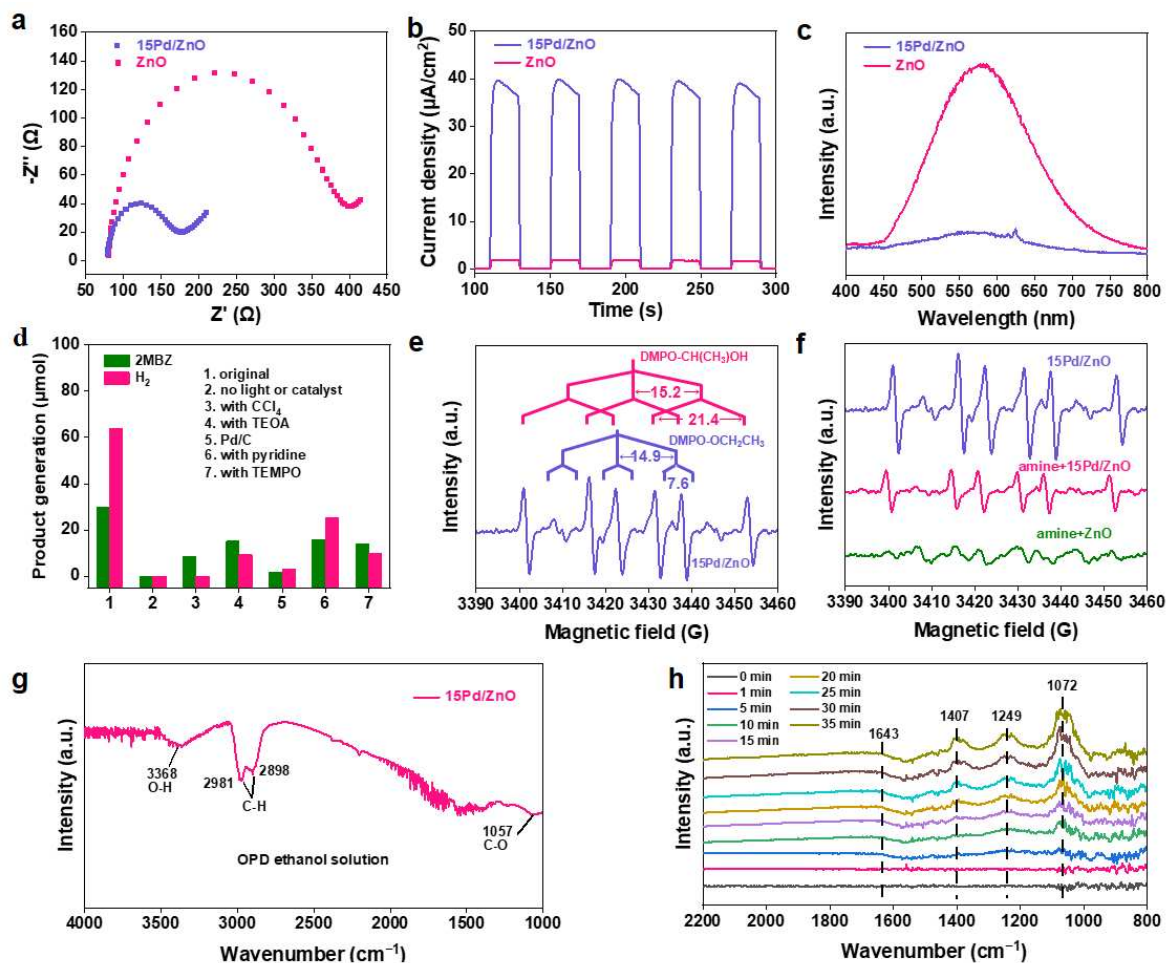
Figure 4. (a) EIS spectra, (b) transient photocurrent spectra and (c) steady-state PL emission spectra of ZnO and 15Pd/ZnO. (d) Photocatalytic performance of control experiments over 15Pd/ZnO after 2 h of illumination. (e) The quantitative analysis result of EPR spectrum of DMPO spin adducts from a reaction from OPD, ethanol and 15Pd/ZnO in Ar-saturated ethanol solution. (f) *In situ* EPR spectra of DMPO spin adducts from a reaction from OPD, ethanol and ZnO or 15Pd/ZnO in Ar-saturated ethanol solution. (g) FT-IR spectrum of OPD ethanol solution adsorbed on 15Pd/ZnO surface. (h) *In situ* FT-IR spectra of photocatalytic synthesis of 2MBZ over 15Pd/ZnO.

introduction of electron scavenger (carbon tetrachloride, CCl_4) into the system completely ceases the H_2 evolution, and the formation of 2MBZ is suppressed after the addition of hole scavenger (triethanolamine, TEOA), revealing that joint participation of photogenerated electrons and holes in the reaction process. Thus, it is further confirming that the significant increase in activity is closely related to the loading of Pd cocatalyst that accelerates the separation/transfer of photogenerated charge carriers. Commercial 10% Pd on carbon (Pd/C) catalyst shows negligible 2MBZ production due to the inability of carbon to generate photogenerated charge,[36] indicating that Pd NPs alone cannot initiate the reaction. When pyridine is introduced into the system, it is adsorbed on the Lewis acid sites of the catalyst surface, resulting in a 47% decrease in the yield of 2MBZ, suggesting that the adsorption of Lewis acid sites is not negligible in the reaction as well.[36] Moreover, it is worth noting that the addition of a radical scavenger (2,6,6-tetramethylpiperidineoxy, TEMPO) suppresses the 2MBZ formation, implying that the formation of 2MBZ proceeds *via* a radical intermediate. The *in situ* electron paramagnetic resonance

(EPR) spectroscopic studies using 5,5-dimethyl-1-pyrroline-N-oxide (DMPO) as a spin-trapping agent under Xe lamp illumination reveal that significant hydroxyethyl radical ($\cdot CH(CH_3)OH$) as well as negligible ethoxy radical ($CH_3CH_2O\cdot$) signals are detected over 15Pd/ZnO in OPD ethanol solution, while only $CH_3CH_2O\cdot$ signal is detected over ZnO (**Figure 4e** and **4f**),[37] implying that the formation of $\cdot CH(CH_3)OH$ is the prerequisite for triggering the reaction. The EPR signal intensity of $\cdot CH(CH_3)OH$ is enhanced over 15Pd/ZnO compared with pristine ZnO, demonstrating that Pd modification favors the α-C−H breakage of ethanol.

In addition, *in situ* Fourier transform-infrared (FT-IR) method is utilized to further elucidate the 2MBZ synthetic pathway. Before the *in situ* FT-IR measurements, 15Pd/ZnO has been subjected to adsorption treatment of OPD ethanol solution for 30 min under Ar atmosphere. The characteristic peaks of ethanol can be observed on the 15Pd/ZnO surface after pretreatment, and no significant characteristic peaks of OPD are detected due to the low concentration of OPD (**Figure 4g**). The peaks at 3368 and 1057 cm^{-1} are assigned to the O−H stretching vibration and the

6

RESEARCH ARTICLE
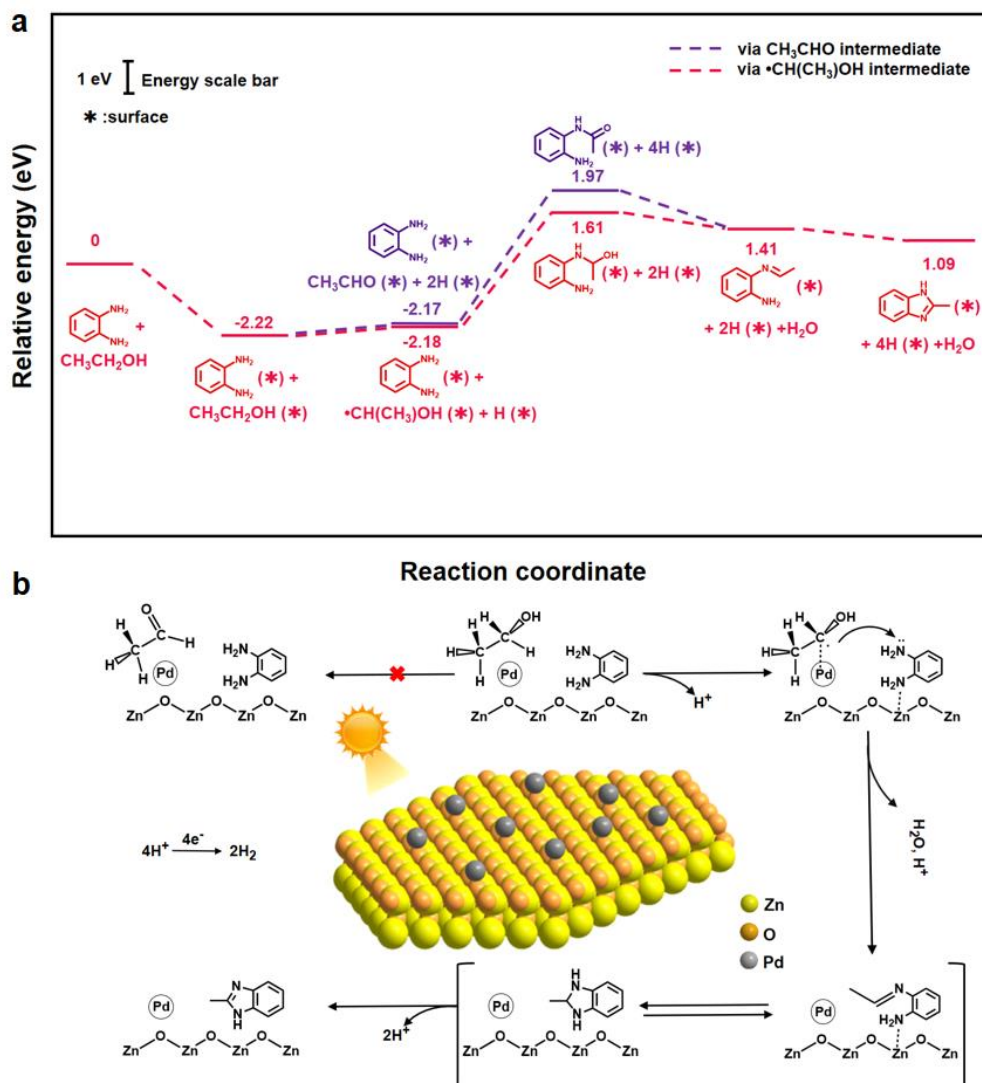
Figure 5. (a) Calculated potential energy diagrams for cross-coupling of OPD and ethanol to 2MBZ catalyzed by Pd/ZnO. (b) Proposed reaction mechanism for photocatalytic 2MBZ synthesis and H_2 evolution over 15Pd/ZnO.

C−O stretching vibration of ethanol, respectively, while the double peaks around 3000 cm^{-1} are ascribed to the C−H stretching vibration of alkyls.[38] In **Figure 4h**, the peaks located at 1643, 1407, 1249 and 1072 cm^{-1} are attributed to C=N bond, C=C bond of benzene ring, C−N bond and C−H bond of alkyl group, respectively, indicating the formation of 2MBZ.[39] Additionally, the characteristic peak of C=O is not detected, expected to be at 1727 cm^{-1}, further proving that ethanol is not converted into acetaldehyde intermediate during the reaction. As expected, our system directly uses the highly reactive •CH(CH$_3$)OH generated by ethanol to participate in the cross-coupling reaction, which is distinctly different from the previously reported mechanism of synthesizing 2MBZ *via* conversion of ethanol to acetaldehyde followed by condensation with OPD.[7, 9d, 9e]

As a comparison and to further learn the unique role of ZnO support, we used the same photodeposition method to modify Degussa P25 (a well-known commercial TiO$_2$ support) to obtain 15Pd/P25 photocatalyst, where Pd NPs with a size of approximately 8.6 nm are distributed on the P25 surface (**Figure S11**). Very interestingly, a large amount of H$_2$ (489 µmol) and the

by-product N-ethyl-2-methylbenzimidazole (NE2MBZ, 22 µmol, see **Figure S12** for the mass spectrum) are generated after 4 h of illumination, implying a 40 and 42% decrease in 2MBZ yield and selectivity, respectively, and a significant amount of acetaldehyde (420 µmol) is detected (**Figure S13**). Furthermore, *in situ* FT-IR spectroscopy also demonstrates that ethanol is converted to acetaldehyde intermediate over 15Pd/P25 during the reaction (**Figure S14**). This is consistent with the previously reported mechanism over TiO$_2$-based photocatalysts,[7] in which acetaldehyde is first produced by dehydrogenation of ethanol, followed by condensation of acetaldehyde with amines to form a Schiff base (see **Figure S15** for the mass spectrum), which readily reacts with a second acetaldehyde molecule leading to the formation of NE2MBZ, meaning that the accumulation of acetaldehyde may affect the selectivity of 2MBZ.[7, 10] In contrast, in our photoredox system (Pd/ZnO), the inductive effect of −C=N− (an electron-withdrawing group) on the Schiff base may affect the nucleophilicity of the neighboring −NH$_2$ group, thereby inhibiting the attack of the •CH(CH$_3$)OH on the neighboring −NH$_2$ group and thus suppressing the formation of by-product NE2MBZ. These

RESEARCH ARTICLE

results clearly show the advantage of the high selectivity toward 2MBZ synthesis by the radical route over Pd/ZnO.

To confirm the above speculated radical route over Pd/ZnO, density functional theory (DFT) calculations have been performed (**Figure S16**). **Figure 5a** illustrates the potential energy diagrams of the reaction paths of •CH(CH$_3$)OH intermediate and acetaldehyde intermediate, respectively. The adsorption steps of ethanol and OPD on Pd/ZnO are both exothermic with values of −0.73 and −1.49 eV, respectively, indicating that the catalyst has a great adsorption capacity for the substrates. The weak dissociation energy makes the dehydrogenation of ethanol to •CH(CH$_3$)OH (0.04 eV) or acetaldehyde intermediate (0.05 eV) is thermodynamically feasible. Subsequently, the reaction of the ethanol-derived intermediates (•CH(CH$_3$)OH or acetaldehyde intermediate) with OPD is endergonic by a high energy barrier, suggesting that the formation of the Schiff base is the rate-limiting step for 2MBZ synthesis. Considering that the reaction energy barrier of •CH(CH$_3$)OH with OPD (3.79 eV) is much lower than that of acetaldehyde (4.14 eV), the more thermodynamically feasible reaction pathway is that the reaction proceeds *via* •CH(CH$_3$)OH intermediate rather than acetaldehyde intermediate, consistent with the conclusion drawn from the experimental results. On the contrary, DFT calculations show that the •CH(CH$_3$)OH over Pd/P25 would spontaneously generate more stable acetaldehyde in thermodynamics (−0.1 eV), thus forming 2MBZ through the reaction of acetaldehyde intermediate with OPD as mentioned in the previous section (**Figures S17** and **S18**).

Taking all the experimental and DFT calculations and analysis into consideration, a plausible photocatalytic reaction mechanism for benzimidazole synthesis concomitantly with H$_2$ production can be proposed (**Figure 5b**). Upon light illumination, photogenerated charge carriers are generated on 15Pd/ZnO. The interfacial interaction between Pd NPs and ZnO NSs facilitates the efficient separation/transfer of photogenerated charge carriers. Unlike the previously reported conversion of ethanol to acetaldehyde followed by condensing with diamines,[7, 9d, 9e] the presence of Pd NPs favors the preferential cleavage of the α-C−H bond of ethanol to generate the highly reactive •CH(CH$_3$)OH, and provides strong adsorption sites for •CH(CH$_3$)OH. On the other hand, the exposed unsaturated metal sites on the 15Pd/ZnO surface act as Lewis acid sites, which are favorable for the adsorption of OPD. Subsequently, the high-reactive •CH(CH$_3$)OH attacks the lone-pair electron of –NH$_2$ group on OPD to generate the Schiff base. Finally, the Schiff base is further dehydrocyclized to form 2MBZ. Meanwhile, the protons extracted by the holes interact with photogenerated electrons and are reduced to H$_2$.

Conclusion

In summary, we report the high-performance photochemical benzimidazoles synthesis integrated with hydrogen (H$_2$) evolution *via* a conceptually new radical-induced dehydrocoupling between *o*-arylenediamines and alcohols over the Pd-decorated ultrathin ZnO nanosheets (Pd/ZnO) photocatalyst. Our system shows great compatibility for various alcohols and *o*-arylenediamines with different functional groups. Distinctly different from the previously reported mechanism for benzimidazoles synthesis by conversion of alcohols to aldehydes followed by condensation with diamines, our mechanistic studies reveal that the unique

advantage of ZnO NSs over other supports and the features of Pd NPs in facilitating the cleavage of the α-C−H bond of alcohols and adsorbing subsequently-generated C−centered radicals give impetus to the coupling reaction between C−centered radicals and *o*-arylenediamines to finally generate benzimidazoles with stoichiometric H$_2$ rather than *via* aldehyde intermediates. This work is expected to present a new horizon to the synthesis of benzimidazoles *via* radical-induced organic coupling reactions and offer instructive guidance on rationally constructing photocatalytic systems for green and sustainable benzimidazoles synthesis integrated with H$_2$ evolution.
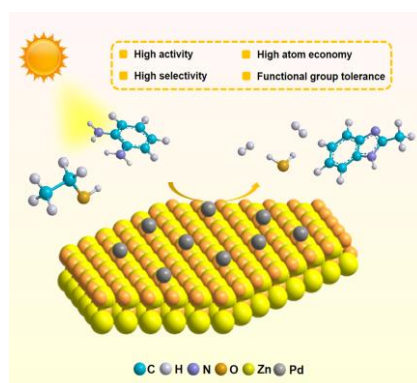
[1]   a) V. V. Fedotov, V. L. Rusinov, E. N. Ulomsky, E. M. Mukhin, E. B. Gorbunov, O. N. Chupakhin, *Chem. Heterocycl. Compd.* **2021**, *57*, 383-409; b) S. Noel, S. Cadet, E. Gras, C. Hureau, *Chem. Soc. Rev.* **2013**, *42*, 7747-7762.

[2]   P. Preston, *Chem. Rev.* **1974**, *74*, 279-314.

[3]   P. L. Beaulieu, B. Haché, E. von Moos, *Synthesis* **2003**, *2003*, 1683-1692.

[4]   Y.-C. Ma, R.-M. Xiong, Y.-Y. Feng, X.-H. Zhang, Y. Xiong, *Tetrahedron* **2020**, *76*, 131474.

[5]   F. F. Stephens, J. D. Bower, *J. Chem. Soc.* **1949**, 2971-2972.

[6]   a) M.-Y. Qi, M. Conte, M. Anpo, Z.-R. Tang, Y.-J. Xu, *Chem. Rev.* **2021**, *121*, 13051-13085; b) J. C. Colmenares, *Curr. Opin. Green Sustainable Chem.* **2019**, *15*, 38-46.

[7]   Y. Shiraishi, Y. Sugano, S. Tanaka, T. Hirai, *Angew. Chem. Int. Ed.* **2010**, *49*, 1656-1660.

[8]   a) M. Jafarpour, F. Feizpour, A. Rezaeifard, N. Pourmorteza, B. Breit, *Inorg. Chem.* **2021**, *60*, 9484-9495; b) W.-K. An, S.-J. Zheng, Y.-N. Du, S.-Y. Ding, Z.-J. Li, S. Jiang, Y.-C. Qin, X.-B. Liu, P.-F. Wei, Z.-Q. Cao, M.-R. Song, Z.-L. Pan, *Catal. Sci. Technol.* **2020**, *10*, 5171-5180; c) B.-C. Luo, Y. Chen, Y.-B. Zhang, J.-Q. Huo, *J. Catal.* **2021**, *402*, 52-60.

[9]   a) A. Eskandari, M. Jafarpour, A. Rezaeifard, M. Salimi, *New J. Chem.* **2018**, *42*, 6449-6456; b) B. Li, R. Tayebee, E. Esmaeili, M. S. Namaghi, B. Maleki, *RSC Adv.* **2020**, *10*, 40725-40738; c) A. Ziarati, A. Badiei, G. Mohammadi Ziarani, H. Eskandarloo, *Catal. Commun.* **2017**, *95*, 77-82; d) Z.-J. Li, Z.-C. Ye, L.-M. Chen, J. Cui, J.-Z. Chen, *ACS Appl. Nano Mater.* **2020**, *3*, 10720-10731; e) Y.-H. Qin, M.-M. Hao, Z.-X. Ding, Z.-H. Li, *J. Catal.* **2022**, *410*, 156-163.

[10]   T. Montini, V. Gombac, J. J. Delgado, A. M. Venezia, G. Adami, P. Fornasiero, *Inorg. Chim. Acta* **2021**, *520*, 120289.

[11]   a) J. M. Narayanam, C. R. Stephenson, *Chem. Soc. Rev.* **2011**, *40*, 102-113; b) C. K. Prier, D. A. Rankic, D. W. MacMillan, *Chem. Rev.* **2013**, *113*, 5322-5363; c) X.-Y. Yu, J.-R. Chen, W.-J. Xiao, *Chem. Rev.* **2021**, *121*, 506-561; d) F.-K. Shang, M.-Y. Qi, C.-L. Tan, Z.-R. Tang, Y.-J. Xu, *ACS Phys. Chem. Au* **2022**, *2*, 216-224; e) Y.-L. Wu, M.-Y. Qi, C.-L. Tan, Z.-R. Tang, Y.-J. Xu, *Chin. J. Catal.* **2022**, *43*, 1851-1859.

RESEARCH ARTICLE

[12] a) Y.-R. Zhu, W.-F. Zhao, J. Zhang, Z. An, X.-D. Ma, Z.-J. Zhang, Y.-T. Jiang, L.-R. Zheng, X. Shu, H.-Y. Song, X. Xiang, J. He, *ACS Catal.* **2020**, *10*, 8032-8041; b) R.-R. Wang, J. Zhang, Y.-R. Zhu, Z.-G. Chai, Z. An, X. Shu, H.-Y. Song, X. Xiang, J. He, *ACS Appl. Mater. Interfaces* **2022**, *14*, 2848-2859; c) D. A. Giannakoudakis, A. Qayyum, M. Barczak, R. F. Colmenares-Quintero, P. Borowski, K. Triantafyllidis, J. C. Colmenares, *Appl. Catal. B* **2023**, *320*, 121939.

[13] Z.-Y. Gao, J.-J. Mu, J. Zhang, Z.-P. Huang, X.-S. Lin, N.-C. Luo, F. Wang, *J. Am. Chem. Soc.* **2022**, *144*, 18986-18994.

[14] S. Hu, X. Wang, *Chem. Soc. Rev.* **2013**, *42*, 5577-5594.

[15] a) J.-H. Zhang, S.-G. Meng, X.-J. Ye, C.-C. Ling, S.-J. Zhang, X.-L. Fu, S.-F. Chen, *Appl. Catal. B* **2017**, *218*, 420-429; b) H. Weerathunga, C. Tang, A. J. Brock, S. Sarina, T. Wang, Q. Liu, H.-Y. Zhu, A. Du, E. R. Waclawik, *J. Colloid Interface Sci.* **2022**, *606*, 588-599.

[16] a) F. Zhang, Y.-H. Li, M.-Y. Qi, Z.-R. Tang, Y.-J. Xu, *Appl. Catal. B* **2020**, *268*, 118380; b) Y.-S. Xie, N. Zhang, Z.-R. Tang, M. Anpo, Y.-J. Xu, *Catal. Today* **2020**, *340*, 121-127.

[17] N. Udawatte, M. Lee, J. Kim, D. Lee, *ACS Appl. Mater. Interfaces* **2011**, *3*, 4531-4538.

[18] J. E. Sutton, D. G. Vlachos, *Ind. Eng. Chem. Res.* **2014**, *54*, 4213-4225.

[19] X. Yin, Y.-Z. Wang, T. H. Chang, P. Zhang, J. Li, P.-P. Xue, Y. Long, J. L. Shohet, P. M. Voyles, Z.-Q. Ma, X.-D. Wang, *Adv. Mater.* **2020**, *32*, 2000801.

[20] a) M.-Y. Qi, H.-K. Wu, M. Anpo, Z.-R. Tang, Y.-J. Xu, *Nano Res.* **2022**, *15*, 9967-9975; b) S. J. Lee, H. J. Jung, R. Koutavarapu, S. H. Lee, M. Arumugam, J. H. Kim, M. Y. Choi, *Appl. Surf. Sci.* **2019**, *496*, 143665.

[21] W. Li, X.-S. Chu, F. Wang, Y.-Y. Dang, X.-Y. Liu, T.-H. Ma, J.-Y. Li, C.-Y. Wang, *Appl. Catal. B* **2022**, *304*, 121000.

[22] B. Coppa, R. Davis, R. Nemanich, *Appl. Phys. Lett.* **2003**, *82*, 400-402.

[23] W. Zhang, X. Jiang, Z.-M. Dong, J. Wang, N. Zhang, J. Liu, G. R. Xu, L. Wang, *Adv. Funct. Mater.* **2021**, *31*, 2107181.

[24] S.-Y. Peng, L.-S. Yang, L.-S. Yu, X.-Y. Li, Y.-Z. Zhou, Y.-Y. Lv, F. Zhu, *New J. Chem.* **2019**, *43*, 18034-18040.

[25] D.-D. Wu, K.-X. Deng, B. Hu, Q.-Y. Lu, G.-L. Liu, X.-L. Hong, *ChemCatChem* **2019**, *11*, 1598-1601.

[26] J. Ni, L.-W. Chen, J.-Y. Lin, S. Kawi, *Nano Energy* **2012**, *1*, 674-686.

[27] L.-L. Wang, S.-F. Ding, P.-Q. Gan, X.-P. Chen, D. Zhang, X.-J. Wei, X.-B. Wang, *React. Kinet. Mech. Catal.* **2016**, *119*, 219-233.

[28] M.-Y. Qi, Y.-H. Li, M. Anpo, Z.-R. Tang, Y.-J. Xu, *ACS Catal.* **2020**, *10*, 14327-14335.

[29] Y. Nosaka, A. Y. Nosaka, *Chem. Rev.* **2017**, *117*, 11302-11336.

[30] Y.-T. Dai, P.-J. Ren, Y.-R. Li, D.-D. Lv, Y.-B. Shen, Y.-W. Li, H. Niemantsverdriet, F. Besenbacher, H.-W. Xiang, W.-C. Hao, N. Lock, X.-D. Wen, J. P. Lewis, R. Su, *Angew. Chem. Int. Ed.* **2019**, *58*, 6265-6270.

[31] X.-Y. Lin, M.-Y. Qi, Z.-R. Tang, Y.-J. Xu, *Appl. Catal. B* **2022**, *317*, 121708.

[32] C.-L. Tan, M.-Y. Qi, Z.-R. Tang, Y.-J. Xu, *Appl. Catal. B* **2021**, *298*, 120541.

[33] M.-Y. Qi, Y.-H. Li, F. Zhang, Z.-R. Tang, Y.-J. Xiong, Y.-J. Xu, *ACS Catal.* **2020**, *10*, 3194-3202.

[34] Y.-H. Li, M.-Y. Qi, Z.-R. Tang, Y.-J. Xu, *J. Phys. Chem. C.* **2022**, *126*, 1872-1880.

[35] J.-Y. Li, M.-Y. Qi, Y.-J. Xu, *Chin. J. Catal.* **2022**, *43*, 1084-1091.

[36] Y.-Z. Chen, Y.-X. Zhou, H.-W. Wang, J.-L. Lu, T. Uchida, Q. Xu, S.-H. Yu, H.-L. Jiang, *ACS Catal.* **2015**, *5*, 2062-2069.

[37] a) S.-J. Xie, Z.-B. Shen, J. Deng, P. Guo, Q.-H. Zhang, H.-K. Zhang, C. Ma, Z. Jiang, J. Cheng, D.-H. Deng, Y. Wang, *Nat. Commun.* **2018**, *9*, 1181; b) S.-F. Jia, X. Shu, H.-Y. Song, Z. An, X. Xiang, J. Zhang, Y.-R. Zhu, J. He, *Ind. Eng. Chem. Res.* **2021**, *60*, 12282-12291.

[38] a) C. Choong, Z.-Y. Zhong, L. Huang, A. Borgna, L. Hong, L.-W. Chen, J.-Y. Lin, *ACS Catal.* **2014**, *4*, 2359-2363; b) M. Iwamoto, M. Tanaka, S. Hirakawa, S. Mizuno, M. Kurosawa, *ACS Catal.* **2014**, *4*, 3463-3469.

[39] S. Wei, H.-X. Zhong, H.-T. Wang, Y.-J. Song, C.-M. Jia, M. Anpo, L. Wu, *Appl. Catal. B* **2022**, *305*, 121032.

9

RESEARCH ARTICLE

Entry for the Table of Contents

We for the first time report a conceptually new, highly efficient radical route for the benzimidazoles synthesis *via* radical-induced cross-coupling of alcohols and *o*-arylenediamines concomitantly with hydrogen (H_2) production over Pd modified ultrathin ZnO NSs (Pd/ZnO) under mild conditions.